Functionalisation of TiO2 nanoparticles with a fluorescent organosilane: A synergy enabling their visualisation in biological cells and an enhanced photocatalytic activity

S. Wintzheimer, E. Genin, L. Vellutini, G. Le Bourdon, M. Kessler, S. Hackenberg, S. Dembski, K. Heuzé

Functionalisation of TiO_2 nanoparticles with a fluorescent organosilane: A synergy enabling their visualisation in biological cells and an enhanced photocatalytic activity

S. Wintzheimer[a,b,*], E. Genin[b,c], L. Vellutini[b,c], G. Le Bourdon[b,c], M. Kessler[d], S. Hackenberg[d], S. Dembski[e,f], K. Heuzé[b,c,**]

[a] University Würzburg, Chair of Chemical Technology of Materials Synthesis, Röntgenring 11, 97070 Würzburg, Germany
[b] Univ. Bordeaux, ISM, UMR-5255, F-33400 Talence, France
[c] CNRS, ISM, UMR5255, F- 33400 Talence, France
[d] University Clinic Würzburg, Department of Oto-Rhino-Laryngology, Plastic, Aesthetic and Reconstructive Head and Neck Surgery, Josef-Schneider-Str. 11, 97080 Würzburg, Germany
[e] Fraunhofer Institute for Silicate Research, ISC, Neunerplatz 2 97082 Würzburg, Germany
[f] University Clinic Würzburg, Department of Tissue Engineering and Regenerative Medicine (TERM), Röntgenring 11, 97070 Würzburg, Germany

Nanoparticles, such as TiO_2 particles, have a great potential for biomedical applications due to their ultra-small size and large specific surface area. However, their detection within cells is to date more than challenging. Thus, implementing fluorescence properties to nanoparticles via their controlled functionalisation with an organic chromophore is an original and efficient strategy to enable their visualization. In this work, a silylated coupling agent bearing a luminescent rhodamine B group was synthesised and grafted on the surface of anatase nanoparticles. The successful functionalisation was demonstrated via zeta potential, dynamic light scattering and diffuse reflectance infrared Fourier transform analyses. Remarkably, the obtained luminescent TiO_2 particles showed an improved photocatalytic activity compared to the pristine nanoparticles. Both, as-synthesised and functionalised TiO_2 nanoparticles samples appear to be non-toxic towards malignant and non-malignant cells. Moreover, the detection of the functionalised particles within cultured cells was proven to be easy and efficient via confocal fluorescence microscopy.

1. Introduction

The small size (< 100 nm) of nanoparticles (NPs) makes them ideal to cross cell or tissue barriers while being large enough to be conjugated to antibodies or drugs. This dual property offers a great opportunity to use them as nano-tools for cell imaging, as drug carriers or therapeutic agents. [1] In the case of TiO_2 NPs, their photocatalytic (PC) properties make them ideal candidates for the photodynamic treatment of dermal tumours such as squamous cell carcinomas. [2–5] The transfer of TiO_2 NPs to biomedical applications requires not only their PC activity and non-toxicity but also a facile detectability. Fluorescence microscopy is an elegant non-destructive and efficient way to detect NPs in cells and to analyse particle interactions with cells. [6–8] The introduction of a fluorescent label into a NP system can be easily achieved via a surface functionalisation with organic dyes. [9–13] While the surface of TiO_2 NPs has often been chemically modified in literature for non-biological applications, [14,15] only a few examples for biological cell applications are described. [6,16,17]

Physical adsorption of dyes onto the NP surface were reported by Choi et al. and Řehoř et al., [15,16] but to avoid uncontrolled physical desorption of the fluorophore, their covalent linkage with the hydroxyl groups of the NP surface appeared as a better strategy. [18–20] Thus, the anchoring group of the fluorophore has to be carefully chosen according to its chemical structure, the NP surface chemical

characteristics and the targeted applications. For the functionalisation of TiO_2 NPs with an organic dye, organosilanes appeared to be the perfect anchoring group. Their silane groups can covalently bind to surficial hydroxyl moieties [21,22] under mild conditions, [23,24] which guarantees the chromophore integrity. Furthermore, the Si-O-Ti bonds are stable in water under mild acidic and basic conditions, which constitute appealing features for biomedical applications.

In the herein presented work, hydrothermally synthesised TiO_2 NPs were functionalised by a silylated coupling agent bearing rhodamine B. The successful grafting of the coupling agent onto the NP surface was characterized via diffuse reflectance infrared Fourier transform (DRIFT), dynamic light scattering (DLS), as well as zeta potential measurements. The optical and PC properties of the obtained fluorescent NP system were also investigated and analysed. Additionally, the cytotoxicity of the functionalised TiO_2 NPs was evaluated in the head and neck squamous cell carcinoma-derived cell line (FaDu) as well as in non-malignant primary human bone marrow-derived mesenchymal stem cells (BMSCs). Finally, fluorescent TiO_2 NPs were successfully and efficiently detected in cells by fluorescence microscopy.

2. Experimental methods

2.1. Materials

Solvents and starting materials for organic and inorganic synthesis were purchased from Acros, Alfa Aesar, Aldrich or Fisher Scientific. 2-[2-(2-methoxyethoxy)ethoxy]acetic acid was technical grade. All other chemical compounds were reagent-grade. Triethylamine (TEA) and isocyanatopropyl-triethoxysilane were purified respectively by distillation over CaH_2 and under dynamic vacuum. All chemicals were used without further purification. Water was deionised before use. All solvents for organic synthesis were used anhydrous. DMF and dioxane were purchased. Others solvents were dried over dehydrating agents and distilled under inert atmosphere: CH_2Cl_2 (CaH_2); EtOH (CaH_2); pentane (Benzophenone, Na).

2.2. Synthesis of TiO_2 NPs

TiO_2 NPs synthesis has already been described in detail elsewhere. [25,26] Briefly, titanium(IV) butoxide, 2-[2-(2-methoxyethoxy)ethoxy] acetic acid and water were used as reactants in a molar ratio of 1.00/1.89/3.33. Water was dropped into the mixture of 2-[2-(2-methoxyethoxy)ethoxy]acetic acid and titanium(IV) butoxide and stirred overnight. All volatile constituents were removed and additional water was added yielding a 12 wt-% amorphous titanium solution. This dispersion was hydrothermally treated in an autoclave for 4 h at 200 °C. The obtained gels were dissolved in water (3 wt-%) and pressure filtrated (0.8 µm membrane).

2.3. Synthesis of the fluorescent silylated coupling agent

The fluorescent silylated coupling agent **4**, and its precursors **1**-**3** were synthesised in 4 steps.

2.3.1. Mono Boc protection of 2,2-(ethylenedioxy)bis(ethylamine)

Di-*tert*-butyl dicarbonate (1 eq., 0.05 mmol, 10.91 g) was dissolved in CH_2Cl_2 (100 mL) and dropwise added to 2,2-(ethylenedioxy)bis (ethylamine) (10 eq., 0.5 mmol, 74.10 g) under strong stirring at 0 °C over 8 h. The reaction batch was then stirred for 16 h at room temperature. Water (300 mL) was added and the product was extracted with CH_2Cl_2 (3 × 50 mL). The combined organic phases were washed with water (3 × 150 mL). The organic phase was dried over $MgSO_4$, filtrated and concentrated under reduced pressure to yield compound **1** (97%) as clear and pale yellow oil. ^{1}H NMR (300 MHz, DMSO-d_6): δ(ppm) = 5.77 (s, 1H, NH), 3.51–3.49 (m, 4H, CH_2), 3.41–3.37 (m, 4H, CH_2), 3.07 (dd, J = 5.9 Hz, 2H, CH_2), 2.80 (s, 2H, NH_2), 2.68 (t, J = 5.7 Hz, 2H, CH_2), 1.38 (s, 9H, CH_3). ^{13}C NMR (ppm): 156.0 (1C, C = O), 78.0 (1C, C), 72.8 (2C, CH_2), 70.0/69.9 (2C, CH_2), 41.51 (1C, CH_2), ~ 40.1 (1C, CH_2 in solvent signal), 29.5 (3C, CH_3). MS $[M+H]^+$ 249.20 *m/z*.

2.3.2. Addition of N-Boc- 2,2′-(ethylenedioxy)diethylamine on rhodamine B isothiocyanate

Compound **1** (1.2 eq., 0.48 mmol, 0.119 g) was dissolved in CH_2Cl_2 (3 mL). Triethylamine (TEA – 1.5 eq., 0.6 mmol, 83.74 µL) was added and the mixture was stirred for 10 min. Rhodamine B isothiocyanate (1 eq., 0.4 mmol, 0.214 g) was dissolved in DMF (3 mL) and added to the reaction batch. The reaction was stirred for 16 h at room temperature in darkness. The crude product was obtained as a powder by complete removal of all volatile compounds under reduced pressure. It was extensively washed with diethyl ether under sonication. The product was dissolved in CH_2Cl_2 (5 mL) and 1 M KOH solution (1 mL) was added. The organic solvent and liberated TEA were removed under reduced pressure and the product was extracted from the water phase with CH_2Cl_2 (3 × 10 mL). The combined organic phases were dried over $MgSO_4$, filtrated and concentrated under reduced pressure to yield compound **2** (94%) as dark violet solid. ^{1}H NMR (300 MHz, DMSO-d_6): δ(ppm) = 8.33-6.11 (m, 9H, CH_{arom}), 5.72 (s, 1H, NH), 3.51 (s, 4H, CH_2), 3.41–3.35 (m, 12H, CH_2), 3.07 (dd, J = 5.5 Hz/10.9 Hz, 2H, CH_2), 2.74-2.71 (m, 2H, CH_2), 1.39 (s, 9H, CH_3), 1.25-1.08 (m, 12H, CH_3). ^{13}C NMR (ppm): 169.7 (1C, C = S), 156.0 (2 C, C = O), 153.2/152.7/149.6/1 9.2 (6C, C), 139.6 (1C, C), 129.0 (2C, CH), 125.3 (3C, C), 123.2 (1C, C), 108.5 (2C, CH), 106.7 (2C, C), 97.3 (2C, CH), 78.1 (1C, C), 69.9 (4C, CH_2), 44.2 (1C, CH_2), 40.1 (1C, CH_2 in solvent signal), 34.8 (4C, CH_2), 30.8 (2C, CH_3), 28.6 (3C, CH_3), 21.4 (1C, CH_3), 12.7 (1C, CH_3). MS $[M+H]^+$ 478.40 *m/z*.

2.3.3. Deprotection of Boc protecting group

Compound **2** (0.45 g) was dissolved in CH_2Cl_2 (25 mL) and gaseous HCl was bubbled through the solution during 15 min. At the end of the reaction the solvent was evaporated under reduced pressure to yield the precipitated compound **3** in salt form as a dark violet solid in quantitative yield. For NMR analysis compound **3** was dissolved in $CDCl_3$ and TEA was added for better solubility. ^{1}H NMR (300 MHz, $CDCl_3$): δ(ppm) = 8.00-6.12 (m, 9 H, CH_{arom}), 3.55 – 3.18 (br/m, 20 H, CH_2), 1.18-1.07 (m, 12 H, CH_3). ^{13}C NMR (ppm): 169.9 (1C, C = S), 155.8 (1 C, C = O), 154.2/153.2/152.4/149.4 (6 C, C), 131.0 (2C, CH), 129.1 (3C, CH), 129.1 (1C, C), 127.8 (1C, C), 108.0 (2C, CH), 106.6 (2C, C), 97.3 (2C, CH), 69.9 (4C, CH_2), 44.9 (2C, CH_2), 44.4 (2C, CH_2), 29.6 (2C, CH_2), 12.6 (4C, CH_3). MS $[M+H]^+$ 648.3 *m/z*.

2.3.4. Synthesis of the silylated coupling agent **4**

Compound **3** (1 eq., 0.208 mmol, 0.15 g) was dispersed in CH_2Cl_2 (6 mL). TEA (15 eq., 3.12 mmol, 435 µL) was added and the mixture was stirred until compound **3** was solubilised. Isocyanatopropyltriethoxysilane (1.2 eq., 0.250 mmol, 61.8 µL) was added and the reaction was stirred at room temperature for 16 h. Afterwards the solvent and excess TEA were evaporated under reduced pressure. The obtained product was washed with pentane (3 × 30 mL). Then, all traces of the solvent were evaporated to yield compound **4** (90%) as purple solid. ^{1}H NMR (300 MHz, $CDCl_3$) : δ(ppm) = 8.03-6.32 (m, 9H, CH_{arom}), 5.73 (s, 2H, NH), 5.36 (s, 1H, NH), 5.12 (s, 1H, NH), 3.79-3.72 (m, 6H, CH_2), 3.64 (dd, J = 7.0 Hz/13.95 Hz, 8H, CH_2), 3.54 (s, 4H, CH_2), 3.44 (t, J = 5.1 Hz, 4H, CH_2), 3.42-3.37 (m, 2H, CH_2), 3.29 (t, J = 5.3 Hz, 2H, CH_2), 3.05 (2H, CH_2), 1.59-1.54 (m, 2H, CH_2), 1.19-1.14 (m, 21H, CH_3), 0.60-0.55 (m, 2H, CH_2). ^{13}C NMR (ppm): 169.9 (1C, C = S), 157.6 (1C, C = O), 155.2 (1C, C = O), 154.2/153.2/152.4/149.4 (6C, C), 131.0 (2C, CH), 129.2 (3C, CH), 129.1 (1C, C), 127.8 (1C, C), 108.0 (2C, CH), 106.6 (2C, C), 97.3 (2C, CH), 70.7/ 70.2 (4C, CH_2), 58.3 (4C, CH_2), 57.9 (3C, CH_2), 44.9 (1C, CH_2), 42.8 (1C, CH_2), 40.0 (1C, CH_2), 23.6 (1C, CH_2), 18.3 (3C, CH_3), 12.5 (4C, CH_3), 7.5 (1C, CH_2). MS $[M+H]^+$ 895.4 *m/z*.

2.4. Grafting of the silylated coupling agent onto TiO_2 NPs

To the synthesised TiO_2 NPs (100 mg) in a mixture of water (3.3 mL) and ethanol (12 mL) 28% ammonium hydroxide in water (0.5 mL) solution was added. Coupling agent **4** (2 µmol/mg particles) was mixed with freshly distilled ethanol (4 mL) and dropped in 50 addition steps into the particles solution under stirring over 2.5 h. Then, the reaction batch was heated up to 40 °C for one hour. After reaction, the samples were centrifuged at 8.000 rpm for 1 h and re-dispersed in water (10 mL). The samples were subsequently dialysed against water (10–20 kDa molecular cut-off including 5 water changes).

2.5. Characterisation

The ^{1}H and ^{13}C NMR spectra were recorded on a Bruker Avance 300 FT NMR spectrometer (^{1}H: 300.13 MHz, ^{13}C: 75.46 MHz). Mass spectra were performed on a QStar Elite Mass Spectrometer equipped with an electrospray ionization source operated in positive ion mode. DRIFTS measurements were conducted on a Thermo Scientific Nicolet 6700 spectrometer equipped with a diffuse reflection unit (Harrick Praying Mantis™). The spectra were recorded by averaging 200 scans from 4000 to 400 cm^{-1} at a resolution of 4 cm^{-1}. All powder samples at a concentration of 1 wt-% were intermixed with calcined KBr and finely ground. Attenuated total reflection (ATR) spectra were recorded on a Thermo Scientific Nicolet iS50 spectrometer with an integrated diamond ATR unit. Each spectrum was acquired in the 4000 to 400 cm^{-1} range at a resolution of 4 cm^{-1}, by coadding 200 scans. ATR spectra were corrected using the Advanced ATR correction algorithm (OMNIC™ software, Thermo Scientific). DLS and zeta potential analyses were carried out on the Malvern Instruments Zetasizer Nano ZS ZEN 3600 in combination with the Multi-Purpose Titrator MPT-2. The measurements were performed at 25 °C for diluted aqueous particle dispersions. The isoelectric points (IEPs) were determined by zeta potential measurements during titration with the help of HCl and NaOH. Photoluminescence (PL) analysis on sample solutions was carried out on a Shimadzu UV-3100. The PC activity of the synthesised samples was assessed via measuring the produced Cl- during the dichloroacetic acid degradation under UV light application as already described before. [26] The only modification was the reduction of the reactor volume and thus, of the measured solution to 0.5 L (water, 100 mg/L NP and 1 g/L dichloroacetic acid).

2.6. Cell culture

The FaDu cell line (established from a hypopharyngeal squamous cell carcinoma) [27] was cultivated in Roswell Park Memorial Institute medium (RPMI 1640, Biochrom AG) supplemented with 10% fetal calf serum (FCS, Linaris), 100 µg/mL streptomycin, 100 U/mL penicillin, 1% 100 mM sodium pyruvate and 1% of a 100-fold concentration of non-essential amino acids (Biochrom AG). The tumour cells were incubated at 37 °C/5% CO_2 in 75 cm^2 flasks, replacing the medium every second day. Before reaching 80% of confluence, cells were passaged by trypsinization (trypsin 0.25%-EDTA 1×; Gibco Invitrogen by life technologies), washed and seeded in new flasks or treatment wells. [28] Human adipose tissue-derived BMSC were isolated from subcutaneous adipose tissue of healthy donors undergoing liposuction for abdominoplasty or gynecomastia surgery. Studies were approved by the local Ethics Committee (12/06) and informed consent was obtained from all individuals included in the study. The isolation procedure was performed as previously described. [29] Expansion medium (DMEM-EM) consisted of Dulbecco's Modified Eagle Medium, 10% FCS), and 1% penicillin/streptomycin (Sigma-Aldrich). Medium was changed daily. When cells reached 70% confluence, they were detached with 0.25% trypsin, resuspended in DMEM-EM and subcultured at a concentration of 2000 cells/cm^2. Cell morphology was analysed by microscopy (Leica DMI 4000B Inverted Microscope, Leica Microsystems) as previously described. [30]

2.7. Cytotoxicity

The cell viability was studied using the MTT colorimetric staining method as described in detail in our recent publication. [25] 10^4 cells were seeded per well in 96-well round bottom plates. They were exposed to particle dispersion at TiO_2 concentrations of 50, 100, 150, and 200 µg/mL. NPs were diluted in cell culture medium (DMEM-EM or RPMI, respectively). Cell culture medium alone without particles served as negative control. Particles exposure was carried out for 24 h. After that the MTT assay was performed as previously described. [24] All cytotoxicity studies were performed on eight technical and three biological replicates. Positive control samples (non-cellular controls) were done and confirmed that there are no interferences between the tested nanomaterials and the biochemical assay reagents. Statistical analysis was performed using Graph Pad Prism software 4. The Wilcoxon test was used to evaluate statistical significance of the mean viability values compared to the untreated control, which was defined to be 100%. Differences were considered statistically significant when the P-value was less than 0.05. For fluorescence microscopy, 100 µL of cell suspension was placed onto a glass slide. After 24 h cells were adherent to the glass and the particle exposure could be performed as described before. Fluorescence microscopy images were recorded on a confocal microscope (SP8, Leica).

3. Results and discussion

3.1. Synthesis of TiO_2 NPs functionalised with a luminescent silylated coupling agent: ***TiO_2@4***

Anatase NPs were hydrothermally synthesised in order to obtain a diameter of around 8 nm. [26] Their chemical and physical properties have previously been reported by our group (including X-ray diffraction, transmission electron microscopy, DLS, zeta potential, nitrogen sorption, IR spectroscopy and thermogravimetric analysis). [26] The NPs were functionalised with the luminescent silylated coupling agent **4** in order to implement luminescent properties to the system. This coupling agent was designed to contain an anchoring group, a spacer moiety and a chromophore. A triethoxysilyl group was selected as anchoring group able to covalently bind to the TiO_2 NP surface. Additionally, a polyethylene glycol-like spacer was introduced between the anchoring site and the chromophore in order to increase the distance between the silyl function and the large, rather rigid structure of the dye. This molecular architecture should guarantee a high grafting efficiency of the coupling agent onto the TiO_2 NPs. [31,32] Additionally, it should enhance the colloidal stability of the functionalised particle in water due to the hydrophilic character of the polyethylene glycol-like spacer. [33,34] A commercial rhodamine derivative was chosen as chromophore because of its high photostability and quantum yield, good chemical and thermal stability, as well as non-toxicity. [16,35] Furthermore, the luminescence (at 576 nm) and absorption (at 554 nm) bands of rhodamine B [36] lie above the wavelength range where TiO_2 strongly absorbs light (< 390 nm). [37,38] The fluorescent coupling agent **4** was obtained after four reaction steps. Its synthetic pathway is described in Fig. 1.

According to an optimized protocol inspired by Simanek [39] the mono-protected diamine product **1** was obtained in almost quantitative yield. Then, rhodamine B isothiocyanate was reacted with the free amine of compound **1**, under basic conditions to provide compound **2** in excellent yield (94%). Afterwards, deprotection of compound **2**'s Boc protecting group by HCl gas provided compound **3** as its ammonium salt in quantitative yield. Then, compound **3** was reacted with triethoxy (3-isocyanatopropyl)silane in the presence of TEA to provide compound **4** without additional purification process.

TiO_2@4 was obtained by grafting compound **4** onto TiO_2 NPs. At

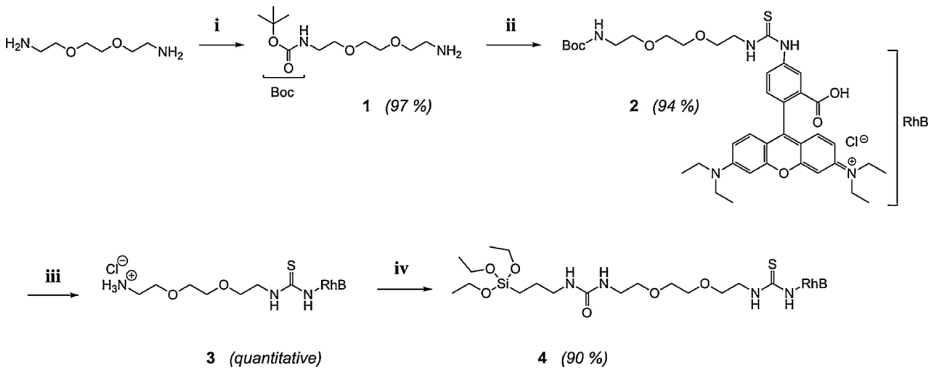

Fig. 1. Synthesis route of the silylated coupling agent **4**. (i) Di-*tert*-butyl dicarbonate, CH_2Cl_2, 0 °C for 8 h and room temperature for 16 h; (ii) rhodamine B isothiocyanate, TEA, CH_2Cl_2/DMF, room temperature, 16 h; (iii) HCl_{gas}, CH_2Cl_2, room temperature, 15 min; (iv) 3-(triethoxysilyl)propyl isocyanate, TEA, CH_2Cl_2, room temperature, 16 h.

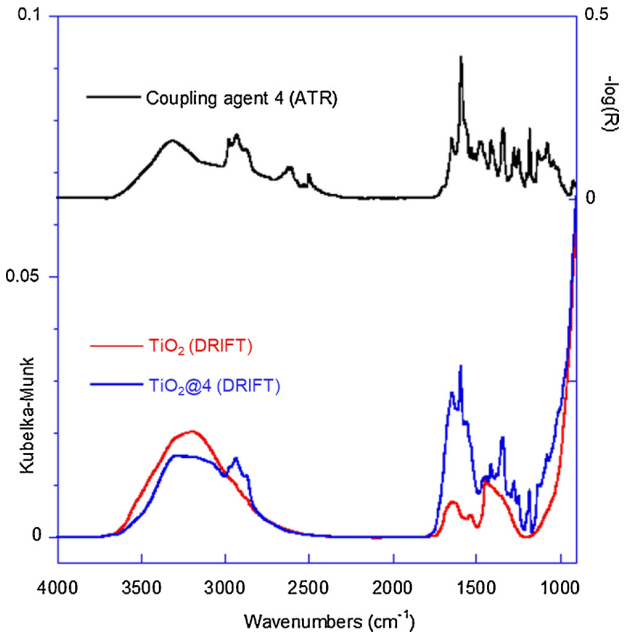

Fig. 2. Experimental DRIFTS spectra (left scale) of unmodified TiO_2 (red) and **TiO_2@4** (blue) and ATR spectrum (right scale) of silylated coupling agent **4** (black) (For interpretation of the references to colour in this figure legend, the reader is referred to the web version of this article).

this stage, it is crucial to avoid the formation of a dense silica layer on the active TiO_2 surface to preserve the PC activity. Therefore, the formation of a silane monolayer on the particles is absolutely necessary. The theoretical amount of silanes yielding a monolayer was calculated to be 1.09 µmol per mg NPs (for more details see Supporting Information). To experimentally verify this calculation and hypothesis, grafting tests with 0.5, 1, 2 and 4 µmol of the commercially available silane N^1-(3-trimethoxysilylpropyl)diethylenetriamine per mg of TiO_2 NPs were conducted (see Table S1 in Supporting Information). The analyses indicated that all silane concentrations from 1 to 4 µmol/mg result in the formation of a monolayer on the NP surfaces. A further condensation onto the surfaces, which would increase the number of silane layers, is indeed hindered by the organic chains of the silanes. Consequently, a concentration of 2 µmol/mg of the silylated coupling agent **4** per NP was chosen for the grafting. It offers a good compromise between using sufficient material to guarantee a successful and efficient grafting even with a larger, bulkier silane and the waste of the silane excess.

3.2. Characterisation of luminescent *TiO_2@4* NPs

TiO_2@4 NPs were characterised via zeta potential, DLS, IR and PL measurements. The pH of the IEP (isoelectric point) was found to be 5.4 while the one of the unmodified TiO_2 NPs was found to be 6.6. This significant pH shift of the IEP indicates the successful chemical surface modification of the TiO_2 NPs. Indeed, the structure of the silylated coupling agent **4** is mainly dominated by the functional groups of rhodamine B. It is thus not surprising that the IEP shifts towards more acidic pH values as the pKa value of rhodamine B is reported to be 3.0–3.7. [40,41] According to these measurements, the highest zeta potential of **TiO_2@4** is reached at basic pHs. Thus, DLS measurements were carried out at a pH of 10 to ensure the best electrostatic stabilisation of the **TiO_2@4** dispersion. Aggregates with diameters of 461 ± 26 nm were measured, which contrast with the dispersibility of the unmodified TiO_2 NPs which was very low at this pH resulting in aggregates with diameters of 10,000 ± 2,000 nm. Nevertheless, the measured hydrodynamic diameter of **TiO_2@4** is still very large compared to an unmodified well-dispersed TiO_2 sample (Supporting Information of [26]) or TiO_2 modified with the commercial amino-silane (Supporting Information, Table S1). This result is most probably caused by the low solubility of rhodamine in water [42] that seems to outbalance the hydrophilic character of the anchoring and spacer moieties and ultimately does not favour an ideal dispersion state of **TiO_2@4**.

3.2.1. IR analysis of luminescent *TiO_2@4* NPs

The characterisation of the modified particles was performed by Diffuse Reflectance Infrared Fourier Transform Spectroscopy (DRIFTS), which is an efficient technique for analysing grafting of particles. [43] The IR spectrum of **TiO_2@4** in comparison to those of the unmodified TiO_2 NPs as well as the ATR spectrum of the silylated coupling agent **4** are depicted in Fig. 2 and Figure S1 (Supporting Information, zoom in the 800-2000 cm^{-1} region). The spectrum of the unmodified TiO_2 NPs shows stretching vibrations of the Ti-O-Ti bond (< 1000 cm^{-1}), [44] as well as stretching and bending vibrations of adsorbed water (~3200 cm^{-1} and 1630 cm^{-1}). [45] Furthermore, stretching vibrations of the carboxylate groups of 2-[2-(2-methoxyethoxy)ethoxy]acetic acid coordinated onto the particles are detected (1347 - 1443 cm^{-1}, 1531 cm^{-1}). [46]

By contrast, the spectrum of **TiO_2@4** is dominated by characteristic absorption bands of the silylated coupling agent **4** proving the successful surface functionalisation. The bands located at wavenumbers from 3080 to 2830 cm^{-1} are due to CH, CH_2 and CH_3 stretching vibrations of the silylated coupling agent **4.** The most intense ones are attributed to the asymmetric stretching vibrations of the CH_3 and CH_2 groups (at 2978 cm^{-1} and 2930 cm^{-1}respectively) and to the symmetric stretching vibrations of CH_2 at 2870 cm^{-1}. The bands observed between 1750 and 1000 cm^{-1} are mainly associated with the rhodamine B component of **4**. However, the assignment of the vibrational modes to the different functional groups of **4** is complex due to the

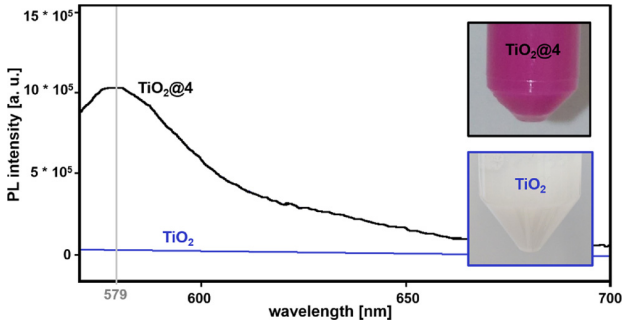

Fig. 3. Photoluminescence spectrum excited at 556 nm showing the fluorescence of **TiO_2@4** compared to unmodified TiO_2. Photographs of both particle samples as dispersions in water at pH = 10 are shown as insets.

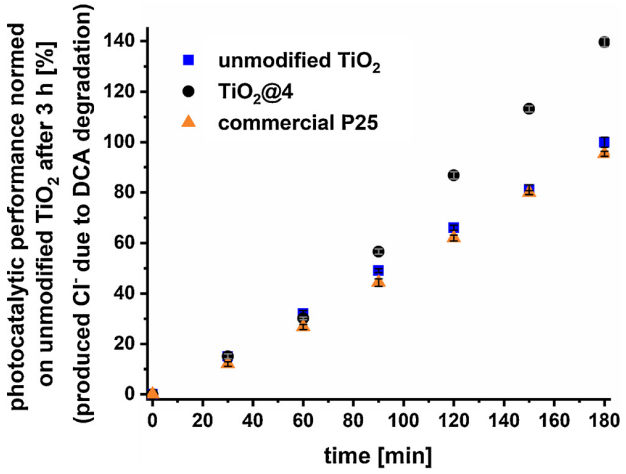

Fig. 4. Photocatalytic performance (SD, n = 3) of **TiO_2@4** in comparison to the unmodified TiO_2 and commercial Aeroxide® P25 TiO_2 NPs determined by the measurement of produced Cl^- anions during the degradation of dichloroacetic acid (DCA). The values are normalised with respect to the amount of degraded DCA by the unmodified TiO_2 sample after 3 h photocatalysis test (= 100%).

presence of coupled modes. Based on literature [47–49], the bands observed at 1645 and 1272 cm^{-1} could be assigned to the xanthene ring stretching vibrations ($\nu_{C=C}$ and $\nu_{C\text{-}O\text{-}C}$) and the band at 1178 cm^{-1} to CCH bending vibrations. Some features can also be assigned to the carboxylate group at about 1580 cm^{-1} (ν_{as} $COO-$) and 1410 cm^{-1} (ν_s $COO-$).

3.2.2. *Photoluminescence and photocatalytic activity of luminescent **TiO_2@4** NPs*

The last evidence of a successful particle modification is the measured PL spectrum and the strong pink colour of the **TiO_2@4** particle sample (Fig. 3).

After having proved the successful synthesis of **TiO_2@4**, its PC activity was examined (Fig. 4). The PC activity of the sample is of great importance for its possible application in photodynamic tumour therapy. For comparison purpose, we also tested the unmodified TiO_2 and commercial Aeroxide® P25 TiO_2 NPs commonly used as benchmarking system. [50–52] As shown in (Fig. 4) the PC activity of **TiO_2@4** is significantly increased even in presence of the grafted silane that could reduce the TiO_2 surface area available for photocatalysis. The most likely explanation of this enhanced PC performance is that the rhodamine acts as a photosensitizer. [53] Dyes in close contact to semiconductor surfaces can transfer absorbed energy and thus lead to the creation of electron-hole pairs that are involved in PC reactions. [54] As rhodamine B absorbs light at a different wavelength range compared to TiO_2, more light is absorbed in total and more electron-hole pairs are created in the **TiO_2@4** system.

3.2.3. *Cell culture studies with **TiO_2@4***

Finally, **TiO_2@4** must demonstrate its biocompatibility in order to be used as photosensitising agent in experimental cancer therapy. Hence, toxicological studies in cell culture were conducted. Both FaDu cells and BMSCs were treated either with unmodified TiO_2 or **TiO_2@4** at different concentrations for 24 h and examined via MTT assay. These cell types were chosen as representative malignant and non-malignant cells, respectively. [2,55] Both particle systems were found to be non-toxic up to 200 µg/mL for stem cells and cancer cells (Fig. 5). It is worth noting that the slight decrease of the cell viability observed in the tumor cell line after exposure to NPs in comparison to the control was categorised as not significant by the statistical analysis (Wilcoxon Test).

Small differences in viability of both cell types towards the two particle samples may be explained by the change of the NPs surface properties. The surface functionalisation changes the IEP of the particles and thus, the surface charge at physiological pH. Furthermore, the coupling agent may certainly modify the polarity of the entire NP system. These variations can impact the NP interaction with cells depending on the cellular model and thus marginally the cell viability.

Besides the biocompatibility of **TiO_2@4** NPs, their efficient detection by confocal microscopy in a cell culture sample was also verified. Representative images of FaDu cells treated with **TiO_2@4** (Fig. 6a) in comparison to FaDu cells without NPs as reference (Fig. 6b) are shown in Fig. 6.

In contrast to pristine FaDu cells, the **TiO_2@4**-treated samples display a strong fluorescent signal originating from the rhodamine B functionality, which is readily detected by the confocal microscope. Thus, this experiment demonstrates the efficient detection of **TiO_2@4** NPs within a cell sample. The fluorescence only comes from the regions where cells are detectable via light microscopy. This result indicates that the NPs are internalised in the cells and not only randomly distributed over the biological sample. This remarkable property of **TiO_2@**

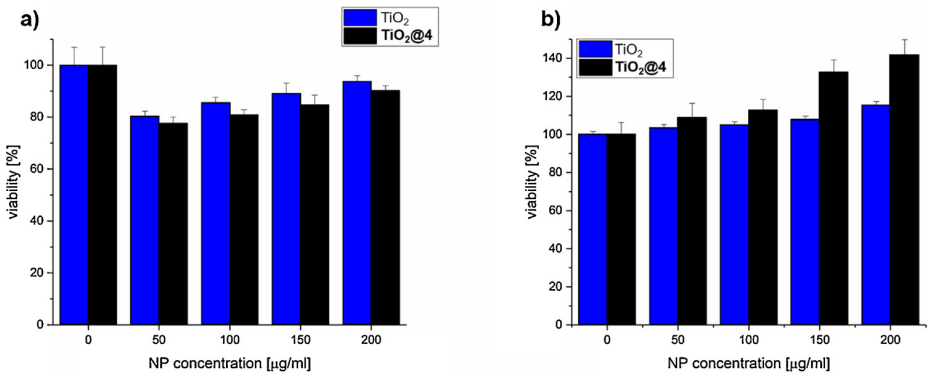

Fig. 5. The viability (SD, n = 8) of malignant cells (a; FaDu) and non-malignant cells (b; BMSCs) treated with TiO_2 and **TiO_2@4** in concentrations of 50–200 µg/mL classifying both NP systems as non-toxic. The values are normalised with respect to the viability of no particle treated cells. For all shown values no significance was found compared to the control system with a p-value < 0.05.

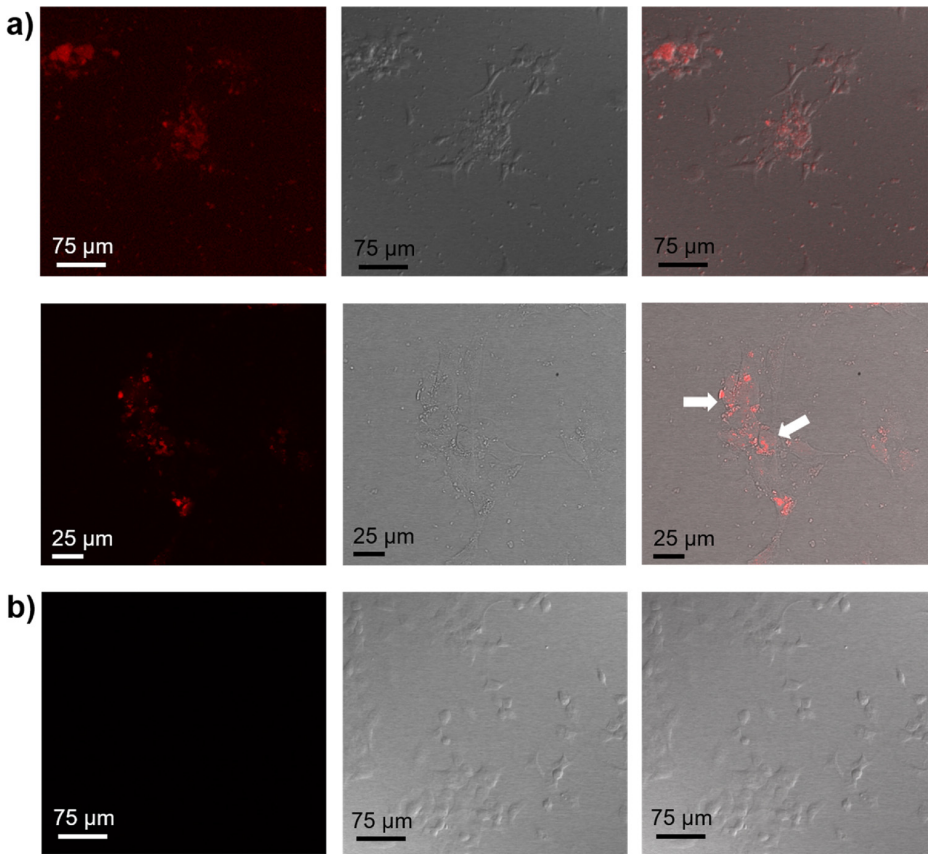

Fig. 6. Confocal fluorescence microscopic images of (a) FaDu cells treated with **TiO_2@4** in two different magnifications and of (b) FaDu cells without NPs as reference. The NPs accumulate only in the cellular cytoplasm and not in the nucleus as shown by the white arrows. From left to right the fluorescence, transmission light and merged images are shown for all cases.

4 NPs may enable a specific detection of marked cells via fluorescence analytic methods. An accurate method to evaluate NP localisation within cells is transmission electron microscopy. However, due to the small size of **TiO_2@4** NPs, it is extremely difficult to discriminate them from cytoplasm structures with this technique and this is why the fluorescence method was rather chosen. Although exact distribution of the NPs in cell organelles is not possible to establish with fluorescence imaging, we can confidently state that the particles accumulate in the cytoplasm in groups of aggregates, while they do not seem to migrate into the cell nucleus.

4. Conclusion

The surface of TiO_2 NPs was successfully functionalised with the silylated coupling agent **4** bearing the chromophore rhodamine B. Remarkably, the surface modification has not diminished but rather increased the PC activity of the TiO_2 NPs. Additionally, the developed **TiO_2@4** was proved to be non-toxic *in vitro* to representative malignant and non-malignant cells, while the NPs were easily detectable in a cell culture sample by fluorescence microscopy. Therefore, this particle system represents a very promising candidate for further studies on the toxicity and cellular uptake of TiO_2 NPs, as well as on the photodynamic treatment of dermal tumours such as squamous cell carcinomas.

Funding sources

This work was financially supported by the University of Bordeaux, France (for SK fellowship) and the Centre National de la Recherche Scientifique (CNRS), France.

Acknowledgments

The authors would like to thank the EU COST action MP1202 for giving networking opportunities associated with this work. Thanks to Dr. Sarah Nietzer (University Clinic Würzburg, Department of Tissue Engineering and Regenerative Medicine) for the acquisition of the confocal fluorescence micrographs.

[1] D. Kim, K. Shin, S.G. Kwon, T. Hyeon, Synthesis and biomedical applications of multifunctional nanoparticles, Adv. Mater. 30 (2018) 1802309, , https://doi.org/10.1002/adma.201802309.
[2] S. Hackenberg, A. Scherzed, W. Harnisch, K. Froelich, C. Ginzkey, C. Koehler, R. Hagen, N. Kleinsasser, Antitumor activity of photo-stimulated zinc oxide nanoparticles combined with paclitaxel or cisplatin in HNSCC cell lines, J. Photochem. Photobiol. B 114 (2012) 87–93, https://doi.org/10.1016/j.jphotobiol.2012.05.014.
[3] F.U. Rehman, C. Zhao, H. Jiang, X. Wang, Biomedical applications of nano-titania in theranostics and photodynamic therapy, Biomater. Sci. 4 (2015) 40–54, https://doi.org/10.1039/C5BM00332F.
[4] M.Z. Iqbal, W. Ren, M. Saeed, T. Chen, X. Ma, X. Yu, J. Zhang, L. Zhang, A. Li, A. Wu, A facile fabrication route for binary transition metal oxide-based Janus nanoparticles for cancer theranostic applications, Nano Res. 11 (2018) 5735–5750, https://doi.org/10.1007/s12274-017-1628-x.
[5] S. Çeşmeli, C. Biray Avci, Application of titanium dioxide (TiO_2) nanoparticles in cancer therapies, J. Drug Target. (2018) 1–5, https://doi.org/10.1080/1061186X.2018.1527338.
[6] K.T. Thurn, T. Paunesku, A. Wu, E.M.B. Brown, B. Lai, S. Vogt, J. Maser, M. Aslam, V. Dravid, R. Bergan, G.E. Woloschak, Labeling TiO_2 nanoparticles with dyes for optical fluorescence microscopy and determination of TiO_2-DNA nanoconjugate stability, Small. 5 (2009) 1318–1325, https://doi.org/10.1002/smll.200801458.
[7] B. Liu, J.F. Rusling, Cancer diagnostics, J. Mater. Chem. B Mater. Biol. Med. 6

(2018) 2507–2509, https://doi.org/10.1039/C8TB90053A.
[8] Y. Cai, W. Si, W. Huang, P. Chen, J. Shao, X. Dong, Organic dye based nanoparticles for Cancer phototheranostics, Small. 14 (2018) 1704247, , https://doi.org/10.1002/smll.201704247.
[9] M.A. Fox, J.K. Whitesell, D. Magde, L.-Y. Zhu, The effect of dye density on the efficiency of photosensitization of TiO_2 films: light-harvesting by phenothiazine-labelled dendritic ruthenium complexes, Molecules. 14 (2009) 3851–3867, https://doi.org/10.3390/molecules14103851.
[10] Y.-C. Chen, T.-Y. Juang, T.-M. Wu, S.A. Dai, W.-J. Kuo, Y.-L. Liu, F.M.C. Chen, R.-J. Jeng, Orderly arranged NLO materials based on chromophore-containing dendrons on exfoliated layered templates, ACS Appl. Mater. Interfaces 1 (2009) 2371–2381, https://doi.org/10.1021/am900499s.
[11] M. Di Paolo, M.J. Roberti, A.V. Bordoni, P.F. Aramendía, A. Wolosiuk, M.L. Bossi, Nanoporous silica nanoparticles functionalized with a fluorescent turn-on spirorhodamineamide as pH indicators, Photochem. Photobiol. Sci. 18 (2019) 155–165, https://doi.org/10.1039/C8PP00133B.
[12] R. Serrano García, S. Stafford, Y. Gun'ko, Recent progress in synthesis and functionalization of multimodal fluorescent-magnetic nanoparticles for biological applications, Appl. Sci. 8 (2018) 172, https://doi.org/10.3390/app8020172.
[13] M.T. Shah, A. Balouch, E. Alveroglu, Sensitive fluorescence detection of Ni^{2+} ions using fluorescein functionalized Fe_3O_4 nanoparticles, J. Mater. Chem. C Mater. Opt. Electron. Devices 6 (2018) 1105–1115, https://doi.org/10.1039/C7TC04298A.
[14] E. Galoppini, Linkers for anchoring sensitizers to semiconductor nanoparticles, Coord. Chem. Rev. 248 (2004) 1283–1297, https://doi.org/10.1016/j.ccr.2004.03.016.
[15] M.J. Choi, T. Smoother, A.A. Martin, A.M. McDonagh, P.J. Maynard, C. Lennard, C. Roux, Fluorescent TiO_2 powders prepared using a new perylene diimide dye: applications in latent fingermark detection, Forensic Sci. Int. 173 (2007) 154–160, https://doi.org/10.1016/j.forsciint.2006.09.014.
[16] I. Řehoř, V. Vilímová, P. Jendelová, V. Kubíček, D. Jirák, V. Herynek, M. Kapcalová, J. Kotek, J. Černý, P. Hermann, I. Lukeš, Phosphonate–titanium dioxide assemblies: platform for multimodal diagnostic–therapeutic nanoprobes, J. Med. Chem. 54 (2011) 5185–5194, https://doi.org/10.1021/jm200449y.
[17] K. Brown, T. Thurn, L. Xin, W. Liu, R. Bazak, S. Chen, B. Lai, S. Vogt, C. Jacobsen, T. Paunesku, G.E. Woloschak, Intracellular in situ labeling of TiO_2 nanoparticles for fluorescence microscopy detection, Nano Res. 11 (2018) 464–476, https://doi.org/10.1007/s12274-017-1654-8.
[18] F. Forato, S. Talebzadeh, N. Rousseau, J.-Y. Mevellec, B. Bujoli, D.A. Knight, C. Queffélec, B. Humbert, Functionalized core–shell Ag@TiO_2 nanoparticles for enhanced Raman spectroscopy: a sensitive detection method for Cu(II) ions, Phys. Chem. Chem. Phys. 21 (2019) 3066–3072, https://doi.org/10.1039/C8CP07504B.
[19] K. Kalyanasundaram, M. Grätzel, Applications of functionalized transition metal complexes in photonic and optoelectronic devices, Coord. Chem. Rev. 177 (1998) 347–414.
[20] A.M. Nauth, E. Schechtel, R. Dören, W. Tremel, T. Opatz, TiO_2 nanoparticles functionalized with non-innocent ligands allow oxidative photocyanation of amines with Visible/Near-Infrared photons, J. Am. Chem. Soc. 140 (2018) 14169–14177, https://doi.org/10.1021/jacs.8b07539.
[21] Y. Nakanishi, T. Imae, Preparation of siloxy focal dendron-protected TiO_2 nanoparticles and their photocatalysis, J. Colloid Interface Sci. 297 (2006) 122–129, https://doi.org/10.1016/j.jcis.2005.10.017.
[22] S. Marcinko, A.Y. Fadeev, Hydrolytic stability of organic monolayers supported on TiO_2 and ZrO_2, Langmuir. 20 (2004) 2270–2273, https://doi.org/10.1021/la034914l.
[23] J. Zhao, M. Milanova, M.M.C.G. Warmoeskerken, V. Dutschk, Surface modification of TiO_2 nanoparticles with silane coupling agents, Colloids Surf. Physicochem. Eng. Asp. 413 (2012) 273–279, https://doi.org/10.1016/j.colsurfa.2011.11.033.
[24] M. Iijima, M. Kobayakawa, H. Kamiya, Tuning the stability of TiO_2 nanoparticles in various solvents by mixed silane alkoxides, J. Colloid Interface Sci. 337 (2009) 61–65, https://doi.org/10.1016/j.jcis.2009.05.007.
[25] S. Koch, M. Kessler, K. Mandel, S. Dembski, K. Heuzé, S. Hackenberg, Polycarboxylate ethers: the key towards non-toxic TiO_2 nanoparticle stabilisation in physiological solutions, Colloids Surf. B Biointerfaces 143 (2016) 7–14, https://doi.org/10.1016/j.colsurfb.2016.03.010.
[26] S. Wintzheimer, W. Szczerba, A. GuilhermeBuzanich, S. Kashiwaya, A. Klein, W. Jaegermann, T. Toupance, A. Shmeliov, V. Nicolosi, K. Heuzé, K. Mandel, S. Dembski, Discovering the determining parameters for the photocatalytic activity of TiO_2 colloids based on an anomalous dependence on the specific surface area, Part. Part. Syst. Charact. 35 (2018) 1800216, , https://doi.org/10.1002/ppsc.201800216.
[27] S.R.S. Rangan, A new human cell line (FaDu) from a hypopharyngeal carcinoma, Cancer. 29 (1972) 117–121, https://doi.org/10.1002/1097-0142(197201)29:1<117::AID-CNCR2820290119>3.0.CO;2-R.
[28] H. Moratin, A. Scherzad, T. Gehrke, P. Ickrath, K. Radeloff, N. Kleinsasser, S. Hackenberg, Toxicological characterization of ZnO nanoparticles in malignant and non-malignant cells: toxicity of ZnO-NPs, Environ. Mol. Mutagen. 59 (2018) 247–259, https://doi.org/10.1002/em.22156.
[29] A. Scherzad, S. Hackenberg, K. Froelich, A. Radeloff, A. Technau, M. Kessler, R. Hagen, K. Rak, C. Koehler, N. Kleinsasser, The effect of wound fluid on adipose-derived stem cells *in vitro* : a study in human cell materials, Tissue Eng. Part C Methods 17 (2011) 809–817, https://doi.org/10.1089/ten.tec.2010.0257.
[30] A. Scherzad, M. Steber, T. Gehrke, K. Rak, K. Froelich, P. Schendzielorz, R. Hagen, N. Kleinsasser, S. Hackenberg, Human mesenchymal stem cells enhance cancer cell proliferation via IL-6 secretion and activation of ERK1/2, Int. J. Oncol. 47 (2015) 391–397, https://doi.org/10.3892/ijo.2015.3009.
[31] L. Mitcova, H. Rahma, T. Buffeteau, R. Clérac, L. Vellutini, K. Heuzé, Dendritic maleimide functionalization of core–shell (γ-Fe_2O_3 /polymer) nanoparticles for efficient bio-immobilization, RSC Adv. 5 (2015) 88574–88577, https://doi.org/10.1039/C5RA17928A.
[32] L. Mitcova, T. Buffeteau, G. Le Bourdon, O. Babot, L. Vellutini, K. Heuzé, Positive dendritic effect on maleimide surface modification of core-shell (γ - Fe_2O_3 /Polymer) nanoparticles for bio-immobilization, Chem. Select. 1 (2016) 4350–4356, https://doi.org/10.1002/slct.201600764.
[33] J. Manson, D. Kumar, B.J. Meenan, D. Dixon, Polyethylene glycol functionalized gold nanoparticles: the influence of capping density on stability in various media, Gold Bull. 44 (2011) 99–105, https://doi.org/10.1007/s13404-011-0015-8.
[34] A.C. Balazs, T. Emrick, T.P. Russell, Nanoparticle polymer composites: where two small worlds meet, Science 314 (2006) 1107–1110, https://doi.org/10.1126/science.1130557.
[35] X.-F. Yang, X.-Q. Guo, Y.-B. Zhao, Development of a novel rhodamine-type fluorescent probe to determine peroxynitrite, Talanta 57 (2002) 883–890.
[36] A.S. Kristoffersen, S.R. Erga, B. Hamre, Ø. Frette, Testing fluorescence lifetime standards using two-photon excitation and time-domain instrumentation: rhodamine B, coumarin 6 and Lucifer yellow, J. Fluoresc. 24 (2014) 1015–1024, https://doi.org/10.1007/s10895-014-1368-1.
[37] S.V. Ingale, P.B. Wagh, A.K. Tripathi, R.S. Srivastav, I.K. Singh, R.C. Bindal, S.C. Gupta, TiO_2-polysulfone beads for use in photo oxidation of rhodamine B, Soft Nanosci. Lett. 02 (2012) 67–70, https://doi.org/10.4236/snl.2012.24012.
[38] Y.R. Dai, L.F. Yin, Enhancement of photocatalytic activity for electrospun C@Ti/anatase fibers by lattice distortion under anisotropic stress, Catal. Sci. Technol. 4 (2014) 456–463, https://doi.org/10.1039/C3CY00730H.
[39] W. Zhang, D.T. Nowlan, L.M. Thomson, W.M. Lackowski, E.E. Simanek, Orthogonal, Convergent Syntheses of Dendrimers Based on Melamine with One or Two Unique Surface Sites for Manipulation, J. Am. Chem. Soc. 123 (2001) 8914–8922, https://doi.org/10.1021/ja0041369.
[40] T. Kasnavia, D. Vu, D.A. Sabatini, Fluorescent dye and media properties affecting sorption and tracer selection, Ground Water 37 (1999) 376–381, https://doi.org/10.1111/j.1745-6584.1999.tb01114.x.
[41] M. Mohammadi, A.J. Hassani, A.R. Mohamed, G.D. Najafpour, Removal of rhodamine B from aqueous solution using palm shell-based activated carbon: adsorption and kinetic studies, J. Chem. Eng. Data 55 (2010) 5777–5785, https://doi.org/10.1021/je100730a.
[42] H.M.H. Gad, A.A. El-Sayed, Activated carbon from agricultural by-products for the removal of Rhodamine-B from aqueous solution, J. Hazard. Mater. 168 (2009) 1070–1081, https://doi.org/10.1016/j.jhazmat.2009.02.155.
[43] E. Siurdyban, T. Brotin, D. Talaga, K. Heuzé, L. Vellutini, T. Buffeteau, Immobilization of cryptophane derivatives onto γ- Fe_2O_3 core–Shell magnetic nanoparticles, J. Phys. Chem. C. 120 (2016) 6583–6590, https://doi.org/10.1021/acs.jpcc.5b12514.
[44] A.M. El-Toni, S. Yin, T. Sato, Control of silica shell thickness and microporosity of titania–silica core–shell type nanoparticles to depress the photocatalytic activity of titania, J. Colloid Interface Sci. 300 (2006) 123–130, https://doi.org/10.1016/j.jcis.2006.03.073.
[45] X. Feng, S. Zhang, X. Lou, Controlling silica coating thickness on TiO_2 nanoparticles for effective photodynamic therapy, Colloids Surf. B Biointerfaces 107 (2013) 220–226, https://doi.org/10.1016/j.colsurfb.2013.02.007.
[46] K. Nakamoto, Applications in Bioinorganic Chemistry, in: Infrared Raman Spectra Inorg. Coord. Compd, John Wiley & Sons, Inc., 2008, pp. 333–402 (Accessed 22 May, 2016), http://onlinelibrary.wiley.com.docelec.u-bordeaux.fr/doi/10.1002/9780470405888.ch3/summary.
[47] L. Wang, A. Roitberg, C. Meuse, A.K. Gaigalas, Raman and FTIR spectroscopies of fluorescein in solutions, Spectrochim. Acta A. Mol. Biomol. Spectrosc. 57 (2001) 1781–1791, https://doi.org/10.1016/S1386-1425(01)00408-5.
[48] M. Majoube, M. Henry, Fourier transform Raman and infrared and surface-enhanced Raman spectra for rhodamine 6G, Spectrochim. Acta Part Mol. Spectrosc. 47 (1991) 1459–1466.
[49] N.O. Mchedlov-Petrosyan, L.A. Fedorov, S.A. Sokolovskii, Y.N. Surov, R.S. Maiorga, Structural conversions of rhodamines in solution, Bull. Russ. Acad. Sci. Div. Chem. Sci. 41 (1992) 403–409.
[50] Y. Li, W. Xie, X. Hu, G. Shen, X. Zhou, Y. Xiang, X. Zhao, P. Fang, Comparison of dye photodegradation and its coupling with light-to-electricity conversion over TiO_2 and ZnO, Langmuir 26 (2010) 591–597, https://doi.org/10.1021/la902117c.
[51] C.M. Teh, A.R. Mohamed, Roles of titanium dioxide and ion-doped titanium dioxide on photocatalytic degradation of organic pollutants (phenolic compounds and dyes) in aqueous solutions: a review, J. Alloys. Compd. 509 (2011) 1648–1660, https://doi.org/10.1016/j.jallcom.2010.10.181.
[52] D.S. Bhatkhande, V.G. Pangarkar, A.A.C.M. Beenackers, Photocatalytic degradation for environmental applications – a review, J. Chem. Technol. Biotechnol. 77 (2002) 102–116, https://doi.org/10.1002/jctb.532.
[53] J. Zhao, T. Wu, K. Wu, K. Oikawa, H. Hidaka, N. Serpone, Photoassisted degradation of dye pollutants. 3. Degradation of the cationic dye rhodamine B in aqueous anionic surfactant/TiO_2 dispersions under visible light irradiation: evidence for the need of substrate adsorption on TiO_2 particles, Environ. Sci. Technol. 32 (1998) 2394–2400.
[54] S. Biswas, V. Sundstrom, S. De, Facile synthesis of luminescent TiO_2 nanorods using an anionic surfactant: their photosensitization and photocatalytic efficiency, Mater. Chem. Phys. 147 (2014) 761–771, https://doi.org/10.1016/j.matchemphys.2014.06.017.
[55] M. Scanu, L. Mancuso, G. Cao, Evaluation of the use of human Mesenchymal Stem Cells for acute toxicity tests, Toxicol. In Vitro 25 (2011) 1989–1995, https://doi.org/10.1016/j.tiv.2011.07.006.